A Circuit, Waveguide, and Spatial Power Combiner for Millimeter-Wave Amplification

Carlos E. Saavedra, *Member, IEEE,* Warren Wright, and Richard C. Compton, *Member, IEEE*

***Abstract*— A new concept for a millimeter-wave amplifier that uses circuit, waveguide, and spatial power combining is demonstrated. The passive array has a free-space-to-microstrip insertion loss below −1.5 dB from 30 to 44 GHz. Small-signal measurements of the active array reveal an average gain of 5 dB from 41 to 46 GHz and a maximum gain of 6.4 dB at 45.6 GHz. Large-signal measurements reveal a linear power gain of 2 dB and an output power of 23.7 dBm at the 1-dB compression point at 44 GHz.**

***Index Terms*— Gratings, power amplifier array, power combining, quasi-optics.**

I. Introduction

MILLIMETER-WAVE solid-state power combiners typically use either printed circuits, waveguide, or quasi-optics [1]–[3] to combine the outputs of multiple devices. In this paper, a novel power combiner that incorporates circuit, waveguide, and spatial power combining is presented. At the circuit level, seven pseudomorphic high electron-mobility transistors (pHEMT's) are power combined in a single integrated circuit amplifier. A parallel-plate waveguide is then used to power combine a row of amplifiers and a tapered grating spatially power combines different rows of amplifiers. The power combiner is shown in Fig. 1.

Incident energy is coupled from free space to a stack of parallel-plate waveguides using a tapered three-dimensional grating. From the parallel-plate guide, there is a transition to a microstrip-based monolithic-microwave integrated-circuit (MMIC) amplifier. The output signal is transitioned back to the parallel-plate waveguide and finally to free space via another tapered grating. The parallel-plate-to-microstrip transition is unique in that it serves the dual function of being a waveguide transition and a power-splitting/combining circuit.

A critical issue in spatial power combining is the efficient coupling of energy from free space to the printed-circuit transmission lines that feed the active elements. Since the array shown in Fig. 1 does not use printed antennas or probes [4]–[9] to couple energy from free space to the printed transmission lines, the insertion loss for the passive system is small and also broad-band. Besides providing a good solution to the free-space-to-microstrip-line coupling problem, the grating design has a number of other advantages. Cascaded multistage amplifiers can be used because there are no restrictions on the longitudinal length of the grating. In addition, the structure can house an $n \times n$ array where n is large, as there are no limits on the overall array size. Input–output isolation is good, as demonstrated by experiments, and mutual coupling between vertical elements is very low because the amplifiers are separated by metallic walls. Furthermore, there is plenty of space on the grating structure for including the dc bias circuitry. Finally, on the issue of heat sinking, the tapered grating array also provides a good solution to this problem: the MMIC's are mounted on copper blocks that are epoxied onto the aluminum plates of the grating, thereby allowing for efficient heat removal.

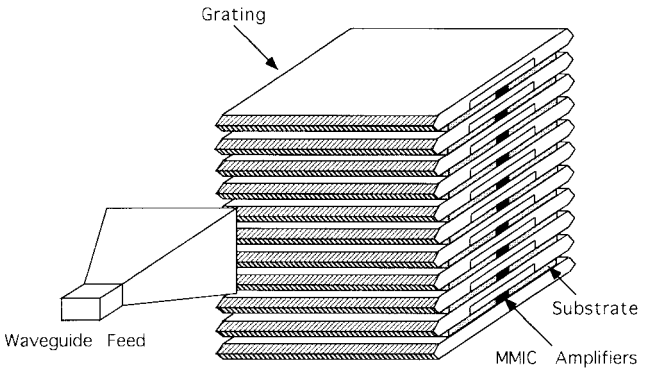

Fig. 1. Millimeter-wave tapered-grating amplifier array. The amplifiers are approximately spaced $\lambda/2$ apart in both the horizontal and vertical dimension at the operating frequency. Lenses (not shown) are used to focus the beam from the waveguide feed to the grating.

II. Three-Dimensional Gratings

Periodic grating structures have been extensively used in millimeter- and submillimeter-wave systems. Some applications include wire grids for polarizers and planar mesh structures for free-space low-pass, bandpass, and high-pass filters [10]–[12]. For those applications, the gratings are typically thin in the direction of propagation. In this section, gratings whose longitudinal dimension span many wavelengths are investigated. The full-wave electromagnetic simulations and experimental measurements reveal that tapered three-dimensional gratings can be designed to have very low transmission loss over large bandwidths because the tapered ends serve as a matching network between the free-space wave impedance and the parallel-plate waveguide impedance.

If a capacitive strip grating is swept in space along the direction of wave propagation, the structure depicted in Fig. 2(a) is obtained. Two main assumptions are needed to determine

Manuscript received July 15, 1998; revised December 1, 1998. This work was supported by the Defense Advanced Research Projects Agency under Grant DAA H04-94G-0087 and by the Army Research Office under Grant DAA G55-97-1-0266.

C. E. Saavedra was with the School of Electrical Engineering, Cornell University, Ithaca, NY 14853 USA. He is now with the Advance Technology Group, Millitech Corporation, South Deerfield, MA 01373-0109 USA.

W. Wright is with the School of Electrical Engineering, Cornell University, Ithaca, NY 14853 USA.

R. C. Compton is with Lucent Technologies, Milpitas, CA 95035-7912 USA.

Publisher Item Identifier S 0018-9480(99)03131-2.

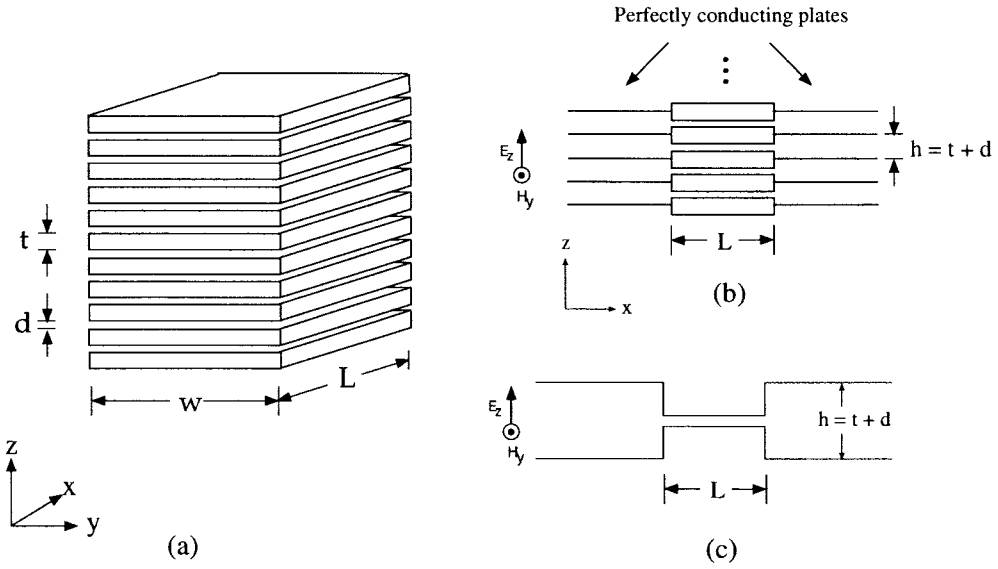

Fig. 2. Thick strip grating. (a) Three-dimensional view. (b) Longitudinal view. (c) Unit waveguide cell. In this paper, $w = 75$ mm, $L = 32$ mm, $t = 3.0$ mm, and $d = 0.4$ mm.

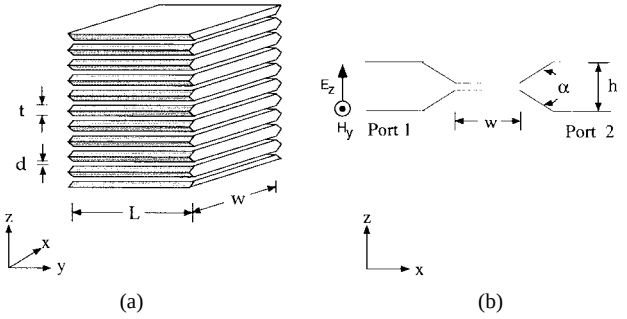

Fig. 3. Tapered Grating. (a) Three-dimensional view. (b) Unit waveguide cell. The flare angle is 20°. The dimensions t, d, w, and L are identical to those of the thick strip grating of Fig. 2.

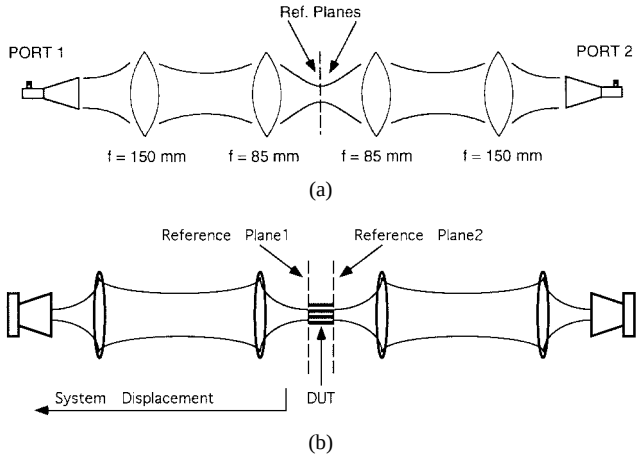

Fig. 4. Gaussian-beam measurement system. A through, short, offset short and load are used to calibrate the system depicted in (a). For wide devices, the reference planes were split by physically moving the left half of the setup, as shown in (b).

the reflection and transmission coefficients of a plane wave normally incident on that grating. The first assumption is that the grating is infinitely periodic, and the second is that the metal strips are of infinite length in the y-direction.

If infinitely thin and perfectly conducting planes are periodically inserted perpendicular to the grating, as in Fig. 2(b), the fields are not disturbed due to the periodic nature of the structure [12]. The grating has now been divided into completely separate, but identical parallel-plate waveguide "cells," one of which is shown in Fig. 2(c). The s-parameters for one of the waveguide cells are identical to the s-parameters of the grating and they can be calculated by mode matching [10], [13] at the waveguide junctions.

A variation on the thick strip grating is shown in Fig. 3(a) in which the grating is tapered at the ends. To compare the behavior of the tapered and thick strip grating, the length of the parallel plates, their thickness, and the period of both gratings were made equal. Thin conducting planes can also be inserted in the tapered grating without disturbing the fields, and the result is the unit waveguide cell shown in Fig. 3(b).

A. Experimental Setup

Before presenting the experimental results, the measurement system will be briefly described. S-parameter measurements from 30 to 50 GHz were made using an HP 8510C Network Analyzer connected to a Gaussian-beam test setup [14]–[18]. Q-band pyramidal horns launch and receive a Gaussian beam and lenses with focal lengths of 85 and 150 mm focus the beam to the device-under-test (DUT), as shown in Fig. 4. To perform two-port measurements on the DUT's, a full two-port calibration procedure was used. The calibration standards used were a through, short, offset short, and load. The short was a polished slab of aluminum mounted on a movable stage controlled by a hand micrometer, and the load was a piece of absorber material.

After calibration, the reference planes are at the middle of the optical setup [Fig. 4(a)]. Since the DUT's are many wavelengths long in the direction of propagation, the reference planes have to be moved to the input and output of the DUT. Since the excitation signals are Gaussian beams and their field intensity changes as a function of distance, it is not possible to

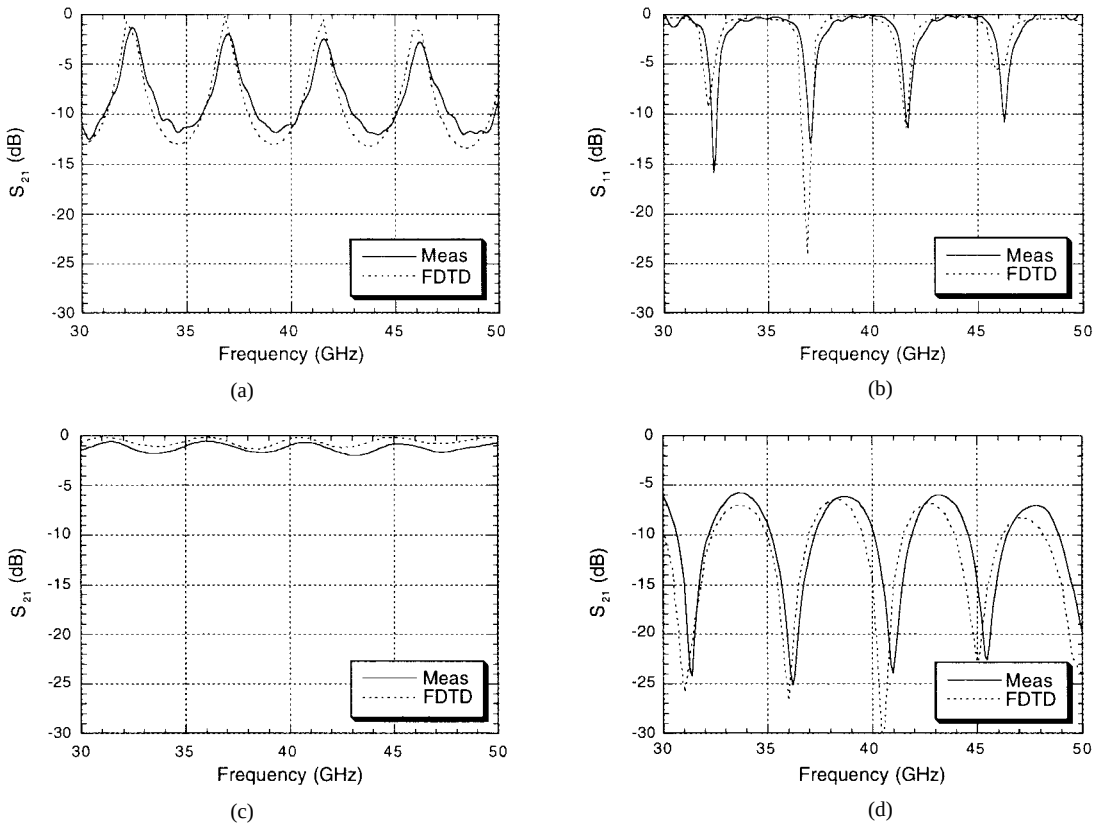

Fig. 5. Measured and calculated scattering parameters for the thick strip grating and the tapered grating. (a) Strip grating S_{21}. (b) Strip grating S_{11}. (c) Tapered grating S_{21}. (d) Tapered grating S_{11}.

use an electrical delay[1] on the HP 8510 to recede the reference planes. The chosen solution was to mount the left half of the setup on a movable stage, as suggested in Fig. 4(b). After calibration, the stage was moved the desired distance and the reference planes were thus split.

B. Strip and Tapered Grating Experimental Results

The gratings shown in Figs. 2(a) and 3(a) were built using aluminum. The dimensions of the gratings were $d = 0.4$ mm, $t = 3.0$ mm, $W = 32$ mm, and $L = 75$ mm. The tapered grating had a flare angle of 20°, making the distance L' between the tips of the tapered edges equal to 48.7 mm. For each grating, 11 aluminum plates were stacked on top of each other with 0.4-mm-thick spacers in between, making the height of the gratings 37 mm.

Fig. 5(a) and (b) shows the measured and calculated s-parameters for the thick strip grating. The theoretical results were obtained using an in-house finite-difference time-domain (FDTD) solver [18]. The measured results were gated using the time-domain features of the HP 8510C vector network analyzer to remove the noise in the data caused by reflections from the lenses after the DUT was inserted and which cannot be calibrated out. An important feature of these plots is the strong resonant behavior observed. The transmission peaks are spaced at 4.6 GHz, corresponding to a resonant length of 32.6 mm, indicating that the resonance is caused by the parallel-plate waveguide cavities in the grating, which are 32-mm long.

[1]HP 8510C Network Analyzer *Operating and Programming Manual*, Hewlett-Packard Company, Santa Rosa, CA, 1991.

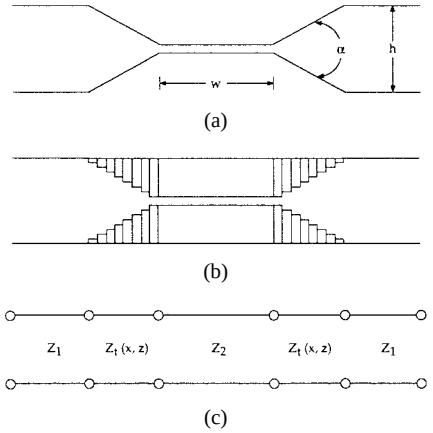

Fig. 6. Tapered grating modeling. (a) Waveguide cell. (b) Tapered regions are approximated by a series of stepped waveguide sections. (c) Transmission-line network.

The s-parameters for the tapered grating are shown in Fig. 5(c) and (d). The transmission and reflection coefficients have dramatically improved over the entire 30–50-GHz range compared with the thick strip grating (Fig. 5). The measured S_{21} is better than -2 dB over the 20-GHz span, setting the bandwidth at 50%. Agreement between the computational and experimental results is typically within a decibel for S_{21} and a few decibels for S_{11}. The difference is attributed to phase slippage [19] and to the coupling efficiency of the horns in the measurement system for the TE_{10} mode to the fundamental Gaussian mode.

The tapered edges have improved the frequency response of the grating because they provide a gradual transition from

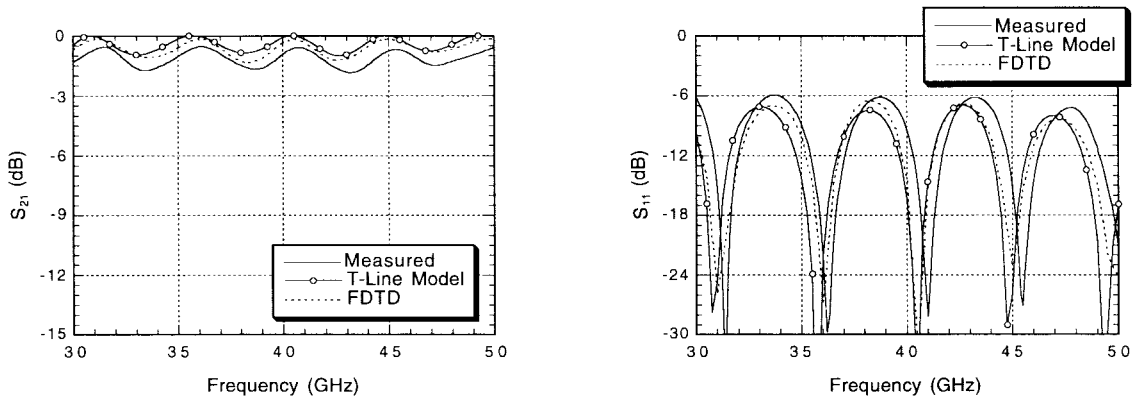

Fig. 7. Tapered grating s-parameters calculated using the transmission-line model. (a) Insertion loss. (b) Return loss.

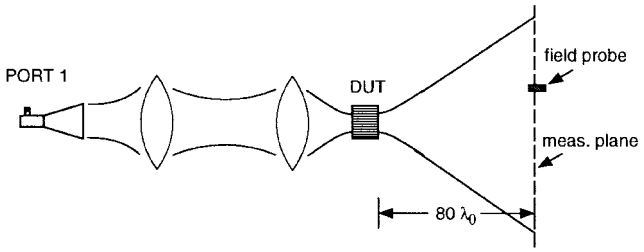

Fig. 8. Far-field measurement setup. A waveguide field probe is used to measure the electric-field magnitude.

the free-space wave impedance to the parallel-plate waveguide impedance. The waveguide model for the tapered grating of Fig. 3(b) can be used to create a transmission-line model for the grating, as shown in Fig. 6(c), and a simple computer program can be used to calculate the s-parameters of the two-port network. A sample s-parameter calculation is shown in Fig. 7, along with experimental and FDTD results for the 20° flare grating. The transmission-line model suggests that a longer taper (i.e., smaller flare angle) will improve the response of the grating because there is a more gradual impedance transition from Z_1 to Z_2. A major advantage of recasting the grating problem in terms of transmission lines is that a variety of grating taper angles can be can be quickly investigated prior to doing a full-wave analysis and building hardware.

C. Tapered Grating Far-Field Measurements

Initially it was not obvious whether the grating would preserve a Gaussian beam as it traveled through the structure. To investigate the interaction of the Gaussian beam with the tapered grating, far-field measurements of the output beam were made using a beam scanner. The experimental setup is depicted in Fig. 8.

The field was sampled using a Q-band waveguide probe. The measurement plane was located at $80\lambda_0$ from the output of the DUT and it encompassed an area of 400 mm in the horizontal direction by 200 mm in the vertical direction. The signal frequency was 40 GHz and beam waist radius was 11.2 mm at the input of the DUT. For reference purposes, the Gaussian beam was first mapped without the tapered grating in the system. Fig. 9(a) shows a gray-scale rendering of the electric-field magnitude for that measurement.

The circular spot of the fundamental Gaussian mode TEM_{00} is clearly seen in Fig. 9(a). The rings observed around the central spot are caused by diffraction from the aperture of the pyramidal horn on the left-hand side of Fig. 8. The far-field plot of the tapered grating output beam is shown in Fig. 9(b). The circular spot in the center of the graph indicates that the input fundamental Gaussian mode has been preserved after traveling through the grating, thus establishing the tapered grating's capability to split a beam and to recombine it again with minimal distortion.

III. Active Amplifier-Array Design

A. Waveguide-to-Microstrip Transitions

Having demonstrated how to couple energy from free-space to parallel-plate waveguide efficiently using a tapered grating, the next step was to design a transition [18], [20], [21] from waveguide to microstrip to guide the energy to the amplifier chips. Fig. 10(a) shows a schematic diagram of the microstrip transitions. To simplify the design process, an infinite array of transitions was assumed. The periodicity of the fields in the structure allows magnetic walls to be inserted in the array, as shown in Fig. 10(b), and the microstrip transitions were designed by considering only one transition.

The width of each transition was 4.24 mm, which was determined primarily by the size of the MMIC's. The MMIC's had a width of 2.66 mm and the spacing between them was 1.58 mm. Impedance Z_1 in Fig. 10(b) is given by $Z_1 = \eta_o d/(w\sqrt{\epsilon_r})$. Using $d = 0.381$ mm, $w = 4.24$ mm, and $\epsilon_r = 3.27$ gives $Z_1 = 18.7\Omega$. The impedance from the overlap region to the beginning of the microstrip transmission lines is also Z_1. The final step in the transition design was to create a broad-band matching network from Z_1 to Z_0, which is the impedance of the microstrip line that fed the MMIC amplifier. The matching network consisted of seven $\lambda/4$ microstrip lines at the design frequency of 44 GHz.

Fig. 11(a) shows the s-parameters for the tapered grating with bare substrates stacked between the plates and Fig. 11(b) shows the s-parameters of the grating with the microstrip transitions. The measurements in Fig. 11(b) reveal that S_{21} is better than -3 dB from 30 to 44.4 GHz, which suggests that only -1.5 dB of power is lost in transitioning from free space to the microstrip circuit lines. To the best of the author's

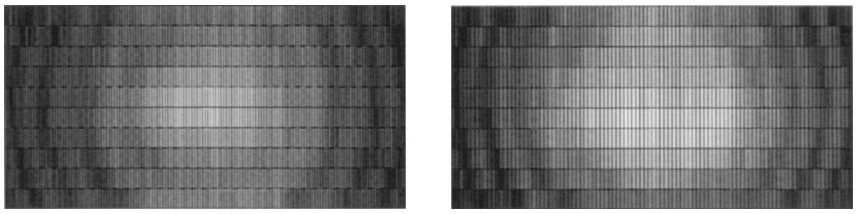

(a) (b)

Fig. 9. Far-field plots. (a) Gaussian beam. (b) Gaussian beam after travelling through the tapered grating.

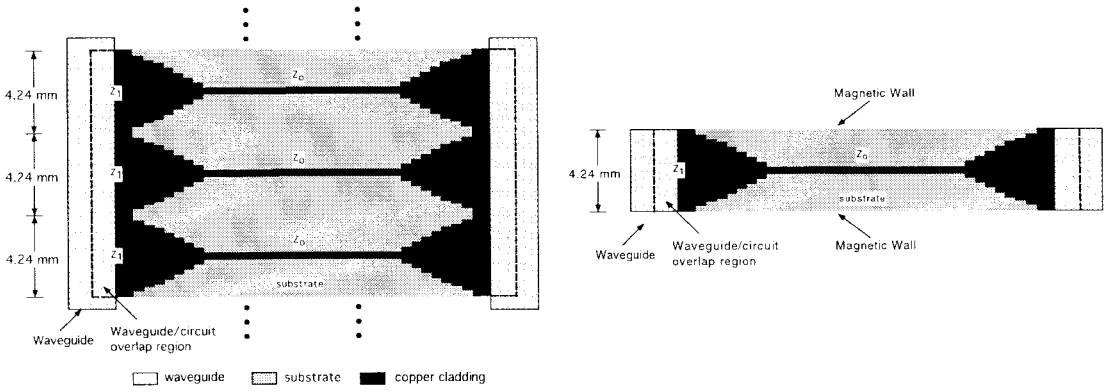

(a) (b)

Fig. 10. (a) Schematic diagram of the parallel-plate waveguide-to-microstrip transitions. (b) Structure is simplified by exploiting its periodicity. The substrate has a relative dielectric constant of 3.27 and a thickness of 0.381 mm.

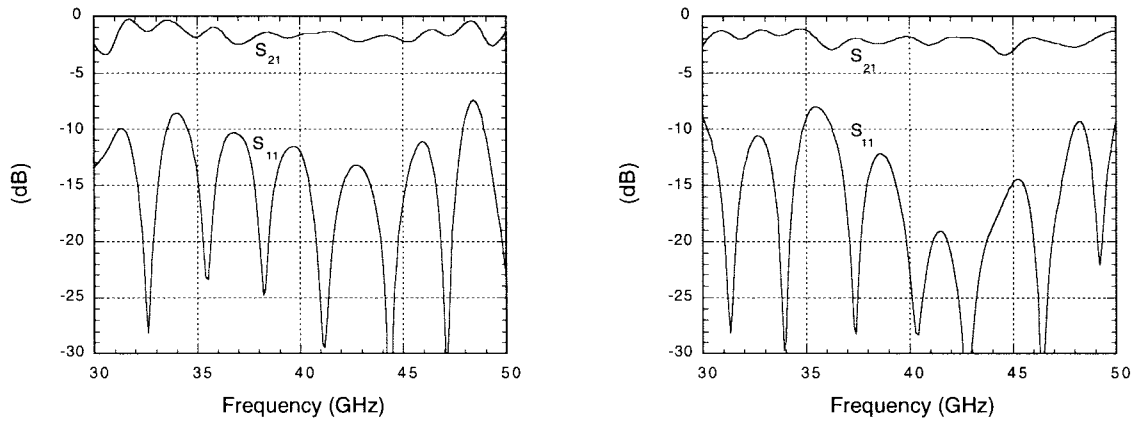

(a) (b)

Fig. 11. (a) Passive tapered grating with unpatterned dielectric substrates. (b) Passive tapered grating with waveguide-to-microstrip transitions. The insertion loss is less than 3 dB over a 14-GHz bandwidth.

knowledge, these are the best passive results for a quasi-optical array at Q-band.

B. Amplifier-Array Assembly

A photograph of the fully assembled tapered grating amplifier array is shown in Fig. 12. A cross-sectional drawing of the array is shown in Fig. 13(a), and a top view drawing is shown in Fig. 13(b). Each row has two separate substrate boards: one at the input and another at the output. Conductive epoxy was applied to the ground plane of the boards in order to attach them onto the grating plates and the positioning holes were used to align the substrate boards prior to curing the epoxy film. For each row of the amplifier array, one power supply was used for the drain bias and one for the gate bias of the MMIC's in that row. Bond wires were used to connect the bias pads together and only one of the bias pads was connected to the power supply. In the grating array, each chip was epoxied onto an individual copper heat-sink chuck, which itself was epoxied onto the grating plates, thus allowing individual MMIC's to be replaced in the event of a malfunction.

IV. Amplifier-Array Results

A. Small-Signal Measurements

A 4×4 AMPLIFIER array was built using Raytheon Electronic's PWR1A power amplifier MMIC [18], [20], [22]. The

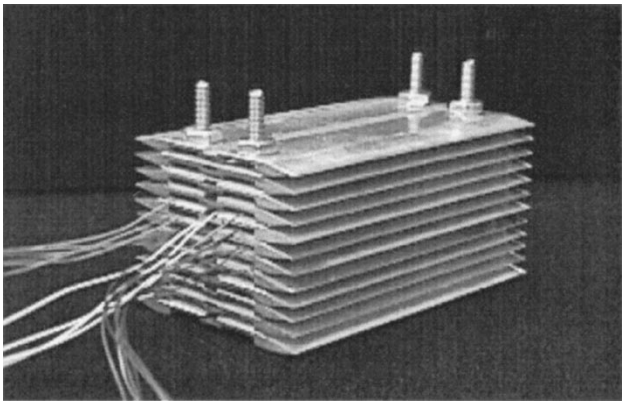

Fig. 12. Tapered-grating amplifier array. The grating plates are pressed together using four threaded screws. The array is 37-mm high, 75-mm wide, and 48-mm long in the direction of propagation.

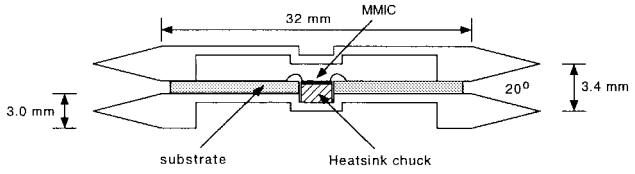

(a)

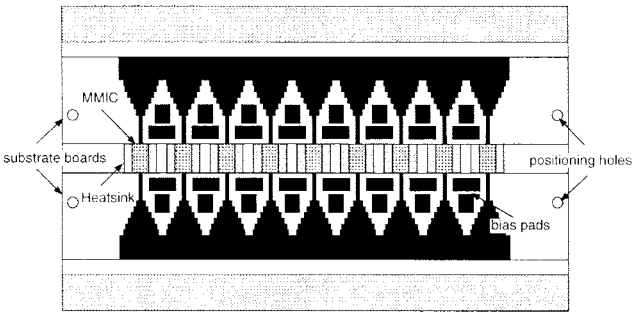

(b)

Fig. 13. Amplifier array layout. (a) Cross-sectional view of one period of the array. (b) Top view of one row of the array.

Raytheon MMIC is a three-stage class-A amplifier, with the first stage using one active device, the second stage two devices, and the last stage four devices, for a total of seven devices per MMIC. The small-signal measurements for the active array using a Gaussian beam of spot radius of 6.5 mm are plotted in Fig. 14(a). The average small-signal gain of the array is about 5 dB, the maximum gain is 6.44 dB at 45.6 GHz, and the bandwidth is 10%. An important issue was the output–input isolation, given by S_{12}, because this will affect the amplifier's stability. In Fig. 14(b) S_{12} is plotted for the array; the isolation is below -30 dB above 41 GHz.

During the measurement process, it was observed that the size of the Gaussian-beam spot had an effect on the results because large beam spots illuminate areas of the array that do not have active elements, thus leading to low gains and high reflection coefficients because the unused microstrip lines in the array are open-circuited. On the other hand, small spot sizes concentrate the energy on the active elements and, therefore, lead to higher values of gain and lower values for the reflection coefficient. To study the effect of the beam spot

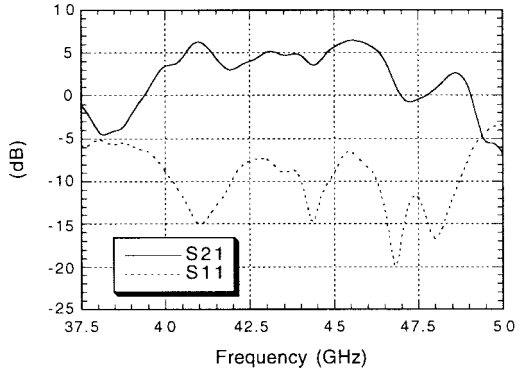

(a)

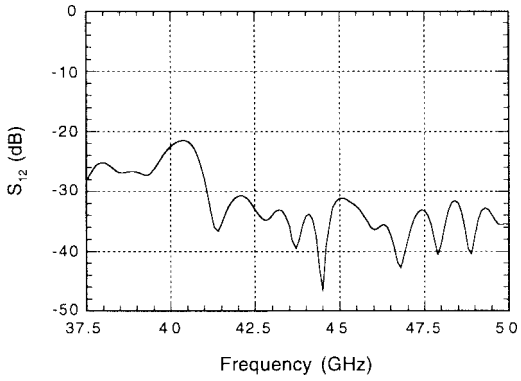

(b)

Fig. 14. S-parameter measurements for the 4 × 4 array. (a) S_{21} and S_{11}. (b) Output–input isolation S_{12}.

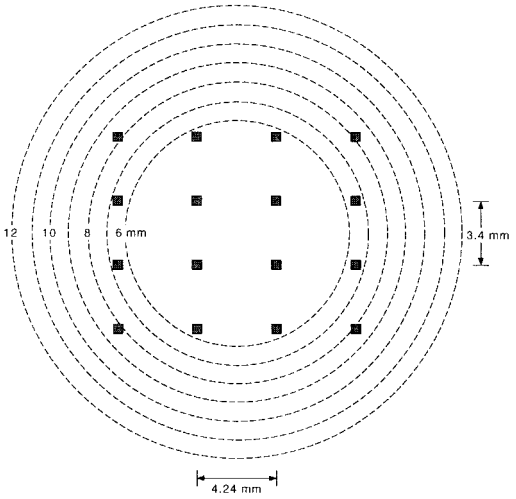

Fig. 15. 4 × 4 array illuminated with beam spots of different radii. The shaded squares represent the amplifier chips inside the grating, and the dashed circles mark the place at which the beam intensity has dropped to 37%.

size on the measured results, the s-parameters of the array were measured using beams with spot radii of 6.5, 7.5, 8.5, 10, and 12 mm (see Fig. 15). In Fig. 16(a) and (b), the gain and reflection coefficients for the array using different beam spots are plotted and, in Fig. 16(c) and (d), the s-parameters are plotted versus beam spot size at two frequency points. As expected, the gain decreases when a larger beam spot is used

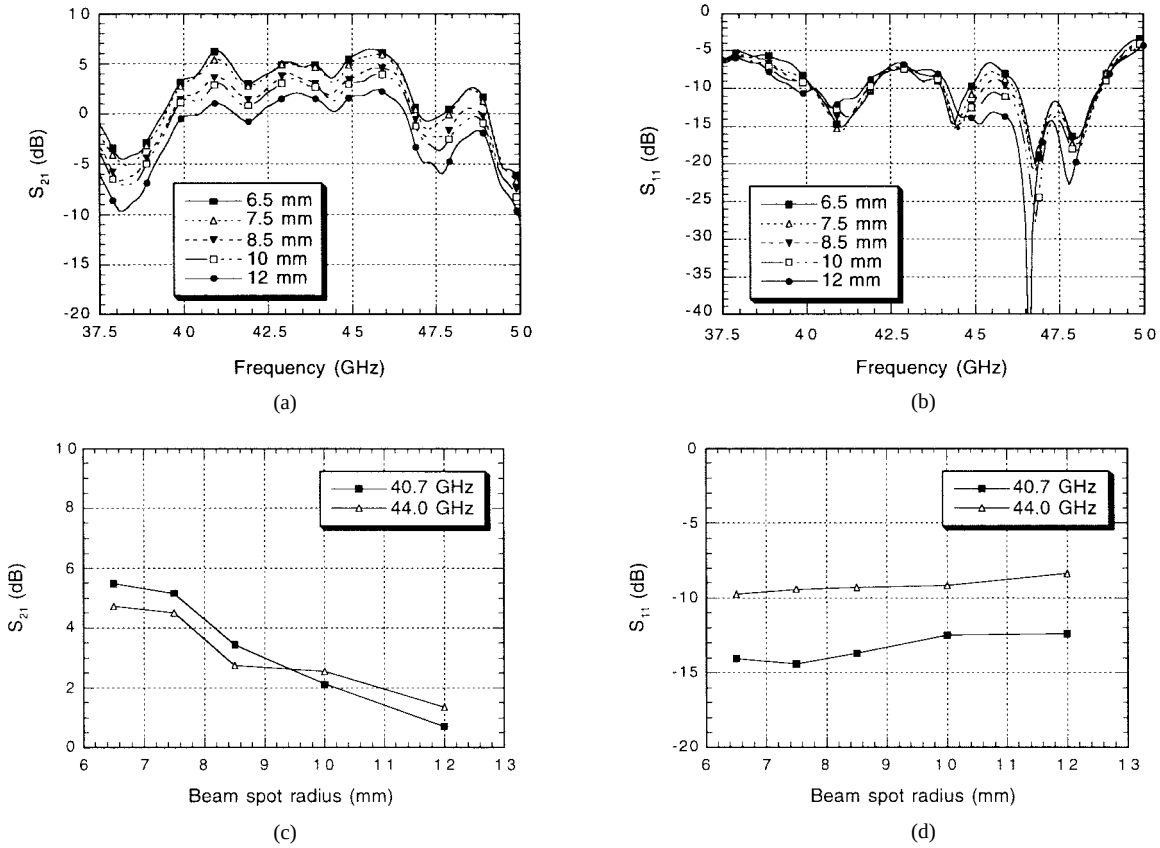

Fig. 16. 4×4 amplifier-array s-parameter variation with beam spot radius. (a) S_{21} and (b) S_{11} versus frequency and (c) S_{21} and (d) S_{11} versus beam radius.

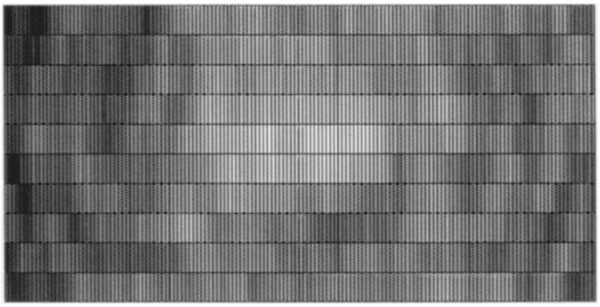

Fig. 17. 4×4 array far-field plot. The amplified beam is distorted toward the right. The measurement was made at 40 GHz over an area of 400 mm by 200 mm at $80\lambda_0$ from the array.

while at the same time the reflection coefficient increases. The impact on S_{21} is more pronounced than on S_{11}: while S_{21} varies between 4 and 5 dB, S_{11} varies by about 2 dB on average. It would seem reasonable to make the spot as small as possible in order to achieve a high gain; however, the spot should not be made arbitrarily small using external dielectric lenses because the beam becomes highly divergent, potentially leading to anomalous results.

The far-field measurement of the output beam of the 16-element array is shown in Fig. 17. Unlike the well-defined central spot seen in Fig. 9(b), the field intensity graph for the amplifier array is noticeably different. The beam has an uneven and asymmetric distribution. A numerical comparison between the far-field plots of Figs. 9(a) and 17 using overlap integrals reveals that only 25% of the energy in Fig. 17 is in the fundamental Gaussian mode, amounting to a 6-dB coupling loss at the receiving horn antenna. Therefore, the actual gain of the array is presumed to be 6 dB higher.

B. Large-Signal Measurements

In addition to small-signal measurements, large-signal or power measurements were made on the tapered grating amplifier array. An impact ionization avalanche transit time (IMPATT) diode source with a nominal output power of 3.4 W at 44 GHz was used as input to the array, and an HP 8487A power sensor connected to an HP EPM-441A power meter was used to measure the output power. A schematic of the power measurement test setup is shown in Fig. 18. The first polarizer is a beam splitter that has a variable angle of polarization θ. Changing the polarizer's angle allows the input power to the DUT to be varied. The second polarizer is oriented at $\theta = 0°$ and its function is to deflect the energy coupled to the cross-polarized mode by the beam splitter out of the system. The third polarizer, also oriented at $\theta = 0°$, is located after the attenuator to ensure that only a vertically polarized mode reaches the receiving horn. The losses in the passive test setup had to be measured in order to determine the true output power of the array. Adding the losses due to the lenses, the attenuator and coaxial cable connecting the receiving horn to the power meter revealed a transmission loss of 25 dB from the output of the DUT to the power sensor. The final step was to determine the incident power (using the power meter) as a function of the polarization angle of the beam splitter.

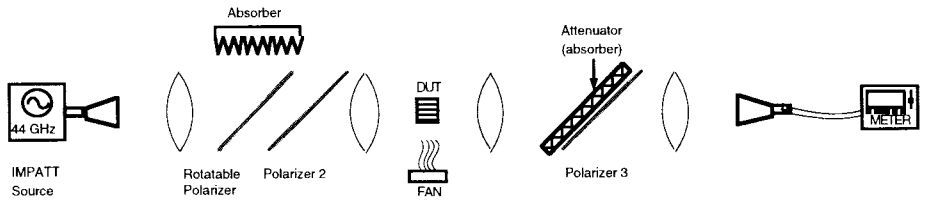

Fig. 18. Top view of the power measurement system. The passive setup was fully characterized using an HP 8510C network analyzer to determine all the losses in the system.

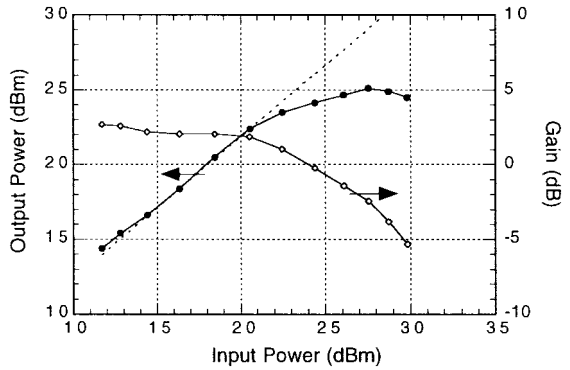

Fig. 19. Output power and power gain versus input power for the tapered grating amplifier array. The dashed line is the extension of the linear gain region.

C. Array Power-Added Efficiency (PAE) and Power Combining

The power measurement results are plotted in Fig. 19. With 13 out of 16 MMIC's operational, the output power of the array at the 1-dB compression point at 44 GHz is 23.7 dBm or 234 mW. The linear power gain of the array is 2.0 dB before it begins to roll off at 21-dBm input power. Each MMIC has a PAE of 20% and a linear power gain of 12 dB. Since the measured power gain of the array was 2.0 dB, the missing 10 dB of gain are accounted for as follows:

bondwire interconnect loss	0.6 dB
passive circuit loss	2.5 dB
coupling loss to standard gain horn	6.0 dB
measurement errors	0.9 dB
TOTAL	10.0 dB.

The PAE of the array will be calculated with and without the 6-dB coupling loss at the receiving horn antenna. The actual *radiated* power is $23.7\ \text{dBm} + 6\ \text{dB} = 29.7\ \text{dBm}$, or $0.93\ \text{W}$, but only 23.7 dBm (234 mW) is captured by the horn antenna. The dc power supplied to the array was 9.36 W and, therefore, its PAE is 10%. When the energy is coupled to the horn antenna, the measured power is 234 mW, as stated before, and, in this case, the PAE is 2.5%. Since the PAE of each MMIC is 20% the available RF power, P_{avail}, from the MMIC's in the array is 1.87 W. Therefore, the power-combining efficiency of the array is $P_{\text{out}}/P_{\text{avail}} = 0.93\ \text{W}/1.87\ \text{W} = 49.7\%$, where P_{out} is the radiated power.

V. Conclusion

The tapered-grating amplifier array demonstrated in this paper makes use of circuit, waveguide, and spatial power combining. The use of a tapered grating to couple energy from the free-space-to-parallel-plate waveguide gives an insertion loss that is less than 1 dB over a 20-GHz span. To couple the energy from the parallel-plate waveguides to the microstrip transmission lines, a novel transition was developed that yields a free-space-to-microstrip insertion loss that is less than 1.5 dB from 30 to 44 GHz. In this manner, the tapered grating array has addressed a key problem in spatial power combining: how to efficiently couple energy from free space to a printed transmission line over a broad bandwidth. The results from the 4×4 active amplifier array reveal an average small-signal gain of 5 dB over a 4.3-GHz span. Due to distortions in the output beam of the array, a significant amount of energy radiated by the amplifier is not coupled to the receiving horn antenna of the measurement system. As a result, it is believed that the actual gain of the array is underestimated by an amount of 6 dB.

Acknowledgment

The authors would like to acknowledge the assistance of G. Swan in machining parts used in used in the experiments.

References

[1] K. J. Russell, "Microwave power combining techniques," *IEEE Trans. Microwave Theory Tech.*, vol. MTT-27, pp. 472–478, May 1979.
[2] K. Chang and C. Sun, "Millimeter-wave power combining techniques," *IEEE Trans. Microwave Theory Tech.*, vol. MTT-31, pp. 91–107, Feb. 1983.
[3] J. W. Mink, "Quasi-optical power combining of solid-state millimeter-wave sources," *IEEE Trans. Microwave Theory Tech.*, vol. MTT-34, pp. 273–279, Feb. 1986.
[4] M. A. Gouker, J. T. Delisle, and S. M. Duffy, "A 16-element subarray for hybrid-circuit tile-approach spatial power combining," *IEEE Trans. Microwave Theory Tech.*, vol. 44, pp. 2093–2098, Nov. 1996.
[5] T. Ivanov and A. Mortazawi, "A two-stage spatial amplifier with hard horn feeds," *IEEE Microwave Guided Wave Lett.*, vol. 6, pp. 88–90, Feb. 1996.
[6] E. A. Sovero, Y. Kwon, D. S. Deakin, A. L. Sailer, and J. A. Higgins, "A pHEMT based monolithic plane wave amplifier for 42 GHz," in *IEEE MTT-S Symp. Dig.*, 1996, pp. 1111–1114.
[7] C.-M. Liu, E. A. Sovero, W. J. Ho, J. A. Higgins, M. P. De Lisio, and D. B. Rutledge, "Monolithic 40-GHz 670-mW HBT amplifier," in *IEEE MTT-S Symp. Dig.*, 1996, pp. 1123–1126.
[8] N. J. Kolias and R. C. Compton, "A monopole-probe-based quasi-optical amplifier array," *IEEE Microwave Theory Tech.*, vol. 45, pp. 1204–1207, Aug. 1997.
[9] J. Dixon, G. O'Dell, J. Schoenberg, S. Duncan, and Z. Popović, "60-GHz monolithic active antenna array," in *IEEE Antennas Propagat. Symp. Dig.*, 1997, pp. 38–41.
[10] R. C. Compton, L. B. Whitbourn, and R. C. McPhedran, "Strip gratings at a dielectric interface and application of Babinet's principle," *Appl. Opt.*, vol. 20, no. 18, pp. 3236–3242, Sept. 1984.
[11] R. C. Compton and R. C. McPhedran, "Bandpass filters: Theory and experiment," *Appl. Opt.*, vol. 22, no. 24, pp. 3920–3921, Dec. 1983.
[12] G. G. MacFarlane, "Quasi-stationary field theory and its application to diaphragms and junctions in transmission lines and wave guides," *Proc. IRE*, vol. 93, pp. 703–719, 1946.
[13] R. E. Collin, *Foundations for Microwave Engineering*. New York: McGraw-Hill, 1966.
[14] D. K. Ghodgaonkar, V. V. Varadan, and V. K. Varadan, "A free-space method for measurement of dielectric constants and loss tangents

at microwave frequencies," *IEEE Trans. Instrum. Meas.*, vol. 37, pp. 789–793, June 1989.
[15] ———, "Free-space measurement of complex permittivity and complex permeability of magnetic materials at microwave frequencies," *IEEE Trans. Instrum. Meas.*, vol. 39, pp. 387–394, Apr. 1990.
[16] V. V. Varadan, R. D. Hollinger, D. K. Ghodgaonkar, and V. K. Varadan, "Free-space, broad-band measurements of high-temperature, complex dielectric properties at microwave frequencies," *IEEE Trans. Instrum. Meas.*, vol. 40, pp. 842–846, Oct. 1991.
[17] N. J. Kolias, "Monopole Probe based millimeter-wave quasi-optical amplifier arrays", Ph.D. dissertation, School Elect. Eng., Cornell Univ., Ithaca, NY, 1996.
[18] C. E. Saavedra-Muñoz, "An integrated millimeter-wave power combiner using three dimensional tapered gratings", Ph.D. dissertation, School Elect. Eng., Cornell Univ., Ithaca, NY, Aug. 1998.
[19] R. J. Wylde, "Millimeter-wave Gaussian beam-mode optics and corrugated feed horns," *Proc. Inst. Elect. Eng.*, vol. 131, pt. H, no. 4, pp. 258–262, Aug. 1984.
[20] C. E. Saavedra, W. Wright, K. Y. Hur, and R. C. Compton, "A millimeter-wave quasi-optical amplifier array using inclined-plane horn antennas," *IEEE Microwave Guided Wave Lett.*, vol. 8, pp. 81–83, Feb. 1998.
[21] C. E. Saavedra, W. Wright, and R. C. Compton, "A passive horn structure with transitions to microstrip for quasi-optical amplifier arrays," presented at the 4th Int. Millimeter- and Submillimeter-Wave Applicat. Conf., San Diego, CA, July 1998.
[22] W. Boulais, R. S. Donahue, A. Platzker, J. Huang, L. Aucoin, S. Shanfield, and M. Vafiades, "A high power Q-band GaAs pseudomorphic HEMT monolithic amplifier," in *IEEE MTT-S Symp. Dig.*, vol. 2, 1994, pp. 649–652.

Carlos E. Saavedra (S'92–M'99) received the B.S. degree (with high distinction) from the University of Virginia, in 1993 and the M.S. and Ph.D. degrees from Cornell University, Ithaca, NY, in 1995 and 1998, respectively, all in electrical engineering. His graduate work included millimeter-wave power combining, millimeter-wave digital modulation circuits, and heterojunction bipolar device fabrication.

He is currently with the Advanced Technology Group, Millitech Corporation, South Deerfield, MA, where he designs millimeter-wave receiver circuits.

Warren Wright was born in Australia. He received the B.Sc. and B.Sc. (with honors) degrees from the University of Queensland, Queens., Australia, in 1980 and 1981, respectively, and the Ph.D. degree in physics from the University of Sydney, Sydney, N.S.W., Australia, in 1990.

He spent three years at the CSIRO Division of Applied Physics, where he performed research in submillimeter lasers, high Tc detectors, and planar array optics. At Cornell University, Ithaca, NY, he has been involved in a number of research projects, including the development of 1-μm-diameter capillary-optical waveguide cells for single molecule laser-induced spectroscopy and the characterization of arrays of antennas and other periodic grid structures, fabricated using e-beam lithography, which operated at visible and near-infrared wavelengths. He is currently a Research Associate in the School of Electrical Engineering, Cornell University. His main research interest is in millimeter-wave quasi-optical systems.

Dr. Wright was the recipient of a three-year Australian Research Council Research Fellowship.

Richard C. Compton (S'84–M'87) received the Ph.D. degree from the California Institute of Technology, Pasadena, CA.

While at Caltech, he worked as a Fulbright Scholar on millimeter and microwave arrays. He is currently an R&D Project Manager with the Wireless Broadband Networks Division, Lucent Technologies, Milpitas, CA, where his group develops products for the wireless delivery of broad-band services to business and residences. His group, formerly part of the Hewlett-Packard Company, was acquired by Lucent in early 1998. The interactive microwave computer-aided design (CAD) package Puff was co-developed by Compton. Over 15 000 copies of Puff have been distributed worldwide. From 1988 to 1996, he served on the faculty of Cornell University. Products that he has helped to design include indoor wireless systems for home lighting control as well as millimeter-wave radios.

Dr. Compton is a National Science Foundation Presidential Young Investigator. He was a member of the FCC's 28-GHz Negotiated Rulemaking Committee in 1994.